Normalized Cuts in 3-D for Spinal MRI Segmentation

Julio Carballido-Gamio, Serge J. Belongie, and Sharmila Majumdar*

***Abstract*—Segmentation of medical images has become an indispensable process to perform quantitative analysis of images of human organs and their functions. Normalized Cuts (NCut) is a spectral graph theoretic method that readily admits combinations of different features for image segmentation. The computational demand imposed by NCut has been successfully alleviated with the Nyström approximation method for applications different than medical imaging. In this paper we discuss the application of NCut with the Nyström approximation method to segment vertebral bodies from sagittal T1-weighted magnetic resonance images of the spine. The magnetic resonance images were preprocessed by the anisotropic diffusion algorithm, and three-dimensional local histograms of brightness was chosen as the segmentation feature. Results of the segmentation as well as limitations and challenges in this area are presented.**

***Index Terms*—Magnetic resonance imaging (MRI), normalized cuts (NCut), Nyström approximation method, segmentation, spine.**

I. Introduction

PHYSICIANS have commonly relied on computed tomography (CT) images to support their decisions in the diagnosis, treatment, and surgery of different pathologies of the spine. CT images have reasonably high-resolution and provide good visualization of bone, however, CT relies on the use of ionizing radiation, and does not depict soft tissue, unlike magnetic resonance imaging (MRI). Thus, registration of CT and MR images of the spine would provide the physicians with more valuable information for diagnostic, therapy, and surgery procedures.

Since the spine experiences nonrigid motion, registration techniques would need to match nondeformable structures prior to utilizing deformable registration tools. In order to facilitate registration of the bony structures, it is important to adequately segment the vertebral bodies.

The segmentation of vertebral bodies is challenging in MRI as variations in soft tissue contrast and radio-frequency (RF) in-homogeneities cause variations in signal intensity across the image, thus increasing the complexity of the segmentation task. Little work has been done in this area, with an initial attempt in [1] to find the boundaries of a vertebral body in MRI cross-sections of the spinal cord.

In this paper, we discuss the segmentation of vertebral bodies from sagittal MR images of the spine using Normalized Cuts (NCut) as the segmentation technique with the Nyström approximation method. NCut formulates segmentation as a graph-partitioning problem: "it maximizes both the total dissimilarity between the different groups and the total similarity within the groups [2]" This segmentation technique readily admits combinations of different features such as brightness, position, windowed histograms, etc., thereby increasing its possible applications to different imaging modalities.

To alleviate the computational demand imposed by NCut, which in principle requires pairwise affinities between all pairs of pixels, we employ the Nyström approximation method, which exploits the fact that there are usually far fewer coherent groups than pixels in a typical image [3]. The Nyström approximation works by solving the grouping problem for a small subset of randomly chosen samples and then extending this solution to the complete set of pixels. The application of the Nyström approximation method to the solution of the eigenvector problem of NCut has already shown encouraging results in areas different than medical imaging [3], [4].

II. Review of Processing Algorithms

A. Review of Normalized Cuts

NCut is an unsupervised segmentation technique developed by Shi and Malik [2] that does not require initialization and has the following three main characteristics:

1) it approaches the segmentation problem as a graph-partitioning problem;
2) it is based on a global criterion;
3) it maximizes both the total dissimilarity between the different groups and the total similarity within the groups.

In NCut, each voxel is considered a node. A measure of dissimilarity between two nodes can be established based on brightness, color, distance, etc. to create an edge. The strength of these edges are weighted with an exponential factor as is shown in (1)

$$w_{ij} = e^{-\frac{d(i,j)}{\sigma_d}} \tag{1}$$

where $d(i,j)$ is the measure of dissimilarity between nodes i and j, and σ_d controls the scale of this measure.

If we have an image $\mathbf{Z}$ with N elements, and we assume a bipartition of $\mathbf{Z}$ into $\mathbf{A}$ and $\mathbf{B}$, where $\mathbf{A} \cup \mathbf{B} = \mathbf{Z}, \mathbf{A} \cap \mathbf{B} = \emptyset$, and $\mathbf{W} \in \mathbb{R}^{N \times N}$ is a symmetric matrix with

$$\mathbf{W}(i,j) = w_{ij} \tag{2}$$

Manuscript received December 17, 2002; revised June 20, 2003. This was supported in part by the National Institute on Aging (NIA) under Grant NIA-RO1-AG17762. The work of J. Carballido-Gamio was supported in part by the University of California under UC-Conacyt and Fulbright scholarships. The Associate Editor responsible for coordinating the review of this paper and recommending its publication was C. Meyer. *Asterisk indicates corresponding author.*

J. Carballido-Gamio is with the Joint Graduate Group in Bioengineering, University of California, San Francisco, and University of California, Berkeley, San Francisco, CA 94143-1290 USA.

S. J. Belongie is with the Department of Computer Science and Engineering, University of California, San Diego, CA 92037 USA.

*S. Majumdar is with the Department of Bioengineering, University of California, Berkeley, CA 94720 USA. She is also with the Departments of Radiology, Orthopedic Surgery, and Growth and Development, University of California, 1 Irving Street, San Francisco, CA 94143-1290 USA (e-mail: majumdar@mrsc.ucsf.edu).

Digital Object Identifier 10.1109/TMI.2003.819929

then

$$\mathrm{cut}(\mathbf{A},\mathbf{B}) = \sum_{u\in\mathbf{A},v\in\mathbf{B}} \mathbf{W}(u,v) \tag{3}$$

and

$$\mathrm{Ncut}(\mathbf{A},\mathbf{B}) = \frac{\mathrm{cut}(\mathbf{A},\mathbf{B})}{\mathrm{assoc}(\mathbf{A},\mathbf{Z})} + \frac{\mathrm{cut}(\mathbf{A},\mathbf{B})}{\mathrm{assoc}(\mathbf{B},\mathbf{Z})} \tag{4}$$

where

$$\mathrm{assoc}(\mathbf{A},\mathbf{Z}) = \sum_{u\in\mathbf{A},p\in\mathbf{Z}} \mathbf{W}(u,p) \tag{5}$$

and similarly for $\mathrm{assoc}(\mathbf{B},\mathbf{Z})$.

In order to maximize both the total dissimilarity between $\mathbf{A}$ and $\mathbf{B}$, and the total similarity within $\mathbf{A}$ and $\mathbf{B}$, Shi and Malik demonstrated in [2] that solving the generalized eigenvector problem

$$\mathbf{W}y = (1-\lambda)\mathbf{D}y \tag{6}$$

and applying a threshold to the eigenvector with the second largest eigenvalue gives the optimal bipartition of the image. In (6), $\mathbf{D}$ is a diagonal matrix such that

$$\mathbf{D}(i,i) = \sum_j \mathbf{W}(i,j) \tag{7}$$

and y is a vector that is function of the group membership indicator vector and $\mathbf{D}$. A detailed description of the method is given in [2].

B. Review of the Nyström Approximation Method Applied to Normalized Cuts

The solution of the eigenvector problem of NCut shown in (6) becomes computationally expensive with large images such as those used in medical imaging (e.g., 256 pixels × 256 pixels or 512 pixels × 512 pixels). Different approaches could be taken to facilitate this solution such as making matrix (2) sparse, so eigensolvers like Lanczos can be used. However, Fowlkes *et al.* demonstrated in [3] that the Nyström approximation method could be applied to give an approximate solution to NCut problem, thus reducing the computational complexity.

The Nyström approximation method solves the grouping problem for a small subset of randomly chosen samples and then extends this solution to the complete set of samples. Fowlkes *et al.* showed in [3] that the diagonalization of (2) can be performed very efficiently using the following approximation to $\mathbf{W}$

$$\hat{\mathbf{W}} = \begin{pmatrix} \mathbf{E} & \mathbf{F} \\ \mathbf{F}^T & \mathbf{F}^T\mathbf{E}^{-1}\mathbf{F} \end{pmatrix} \tag{8}$$

where $\mathbf{E}\in\mathbb{R}^{m\times m}$, $\mathbf{F}\in\mathbb{R}^{m\times n}$, m is the number of randomly chosen samples, $m+n=N$ and $m \ll n$. Here, $\mathbf{E}$ represents the set of weights amongst the randomly chosen samples, $\mathbf{F}$ is the set of weights from the randomly chosen samples to the rest of the nodes, and $\mathbf{F}^T\mathbf{E}^{-1}\mathbf{F}$ approximates the set of weights between the rest of the nodes. When $\mathbf{W}$ is low rank, as in the case when the number of groups is relatively small, this approximation is very close to the exact solution. With a slight modification, the same approximation can be applied to the normalized affinity matrix $\mathbf{D}^{-1/2}\mathbf{W}\mathbf{D}^{1/2}$. A detailed description of the method is provided in [3] and [5].

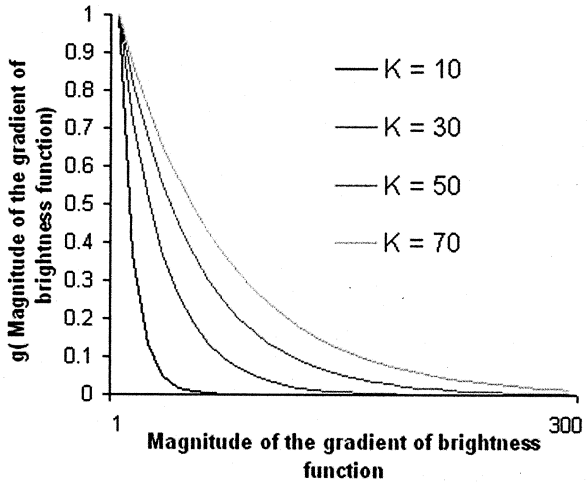

Fig. 1. Shape of $g(\cdot)$ employed in this paper for different values of K.

C. Review of Anisotropic Diffusion

The primary objective of anisotropic diffusion is to smooth images with no distortion of the edges in an image such that at all scales, intra-region smoothing occurs preferentially over inter-region smoothing [6], [7], and to satisfy the causality and immediate localization criteria. In the anisotropic diffusion equation

$$\mathbf{I}_t = c(x,y,t)\nabla^2\mathbf{I} + \nabla c\cdot\nabla\mathbf{I} \tag{9}$$

where $c(x,y,t)$ is the conduction coefficient, t is the scale variable, ∇ and ∇^2 represent the gradient, and Laplacian operators with respect to the space variables, the objective is to assign a value of 1 to the conduction coefficient inside of each region, and 0 at the boundaries.

Setting the conduction coefficient as a function of the magnitude of the gradient of brightness function as suggested by Perona and Malik in [6], provides a good estimate of the edge positions

$$c(x,y,t) = g(\|\nabla\mathbf{I}(x,y,t)\|) \tag{10}$$

where g should be smooth and $g(\cdot)$ is restricted to a subclass of the monotonically decreasing functions. Fig. 1 shows the function $g(\cdot)$ that was used in this study

$$e^{-\frac{\|\nabla\mathbf{I}\|}{K}}, \tag{11}$$

while Fig. 2 shows an scale-space example.

III. MATERIALS AND METHODS

A. Magnetic Resonance Imaging

Sagittal MR images of the spine of six subjects were obtained at 1.5 T (Signa scanner; GE Medical Systems, Milwaukee, WI) using a phased array surface coil. Patients were placed supine in the MR scanner and T1-weighted images were acquired with the following parameters: $\mathrm{TR} = 500$ ms, $\mathrm{TE} = 14$ ms, $\mathrm{flip\ angle} = 90°$, pixel resolution of 0.9375 mm × 0.9375 mm × 5.0 mm, matrix size of 256 pixels × 256 pixels, and slice spacing of 1.0 mm.

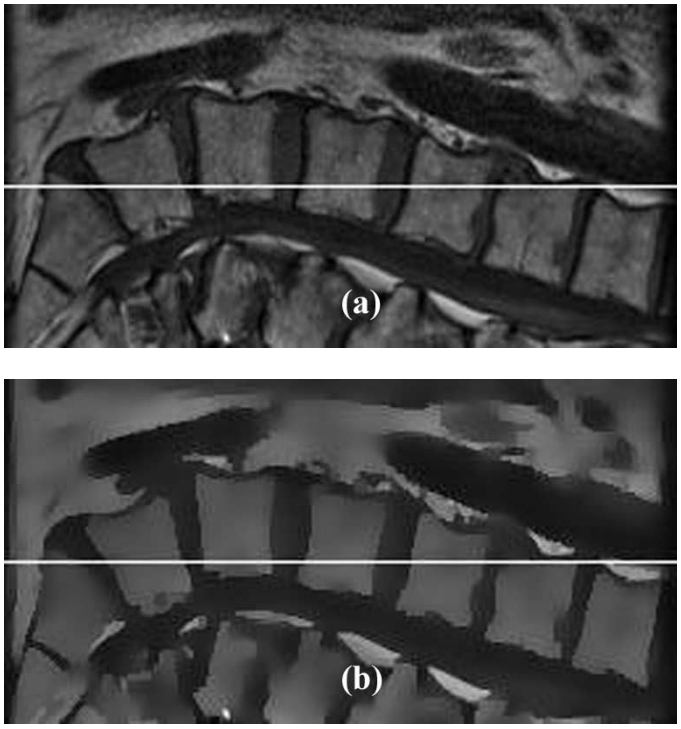

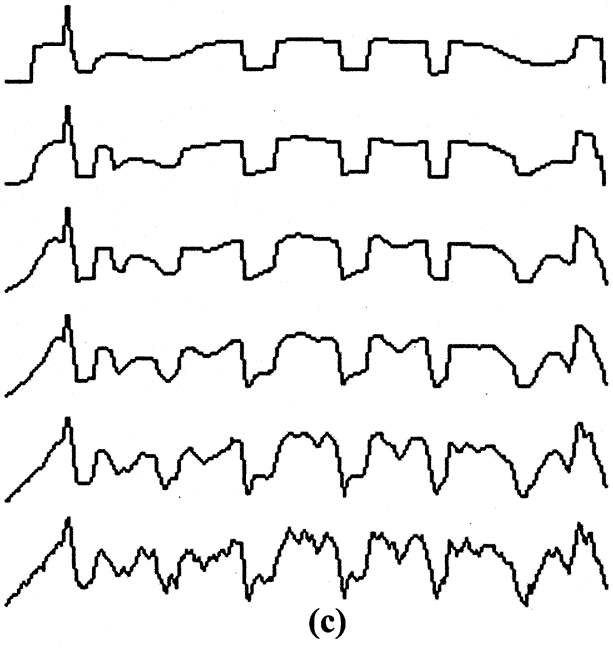

Fig. 2. (a) Cropped coil corrected image. (b) Cropped coil-corrected image with anisotropic diffusion enhancement ($\lambda = 0.25, K = 50, 40$ iterations). (c) Scale-space obtained through the white line with (from bottom to top) zero (original), 5, 40, 100, and 250 iterations with $\lambda = 0.25$ and $K = 50$.

Fig. 3. Cropped image (a) before, and (b) after coil-correction and anisotropic diffusion enhancement ($\lambda = 0.25, K = 50, \text{number of iterations} = 5$).

B. Segmentation of Vertebral Bodies

The acquired slices were coil-corrected and the spacing between them was filled out to create a three–dimensional (3-D) stack. Slices were enhanced through an anisotropic diffusion algorithm, and the slice that showed better the spinal canal was selected for segmentation of its vertebral bodies. Histograms around a local volume surrounding each voxel of the slice of interest were calculated. A measure of histogram similarity was applied to the calculated histograms, and the eigenvector problem of NCut was solved through the Nyström approximation method based on this latest measure.

1) Coil Correction: Since the coil reception profile in phased array surface coils is not homogenous, an intensity-correction algorithm based on division by an edge completed low-pass filtered version of the original image [8] was applied

$$\text{corrected\_image} = \frac{\text{image}}{\text{low\_pass(image)}} \tag{12}$$

where corrected_image is the image after intensity-correction.

2) Interpolation Between Slices: As MR images were acquired with 1.0-mm slice spacing, the slices were interpolated in order to generate a 3-D stack. The interpolated slices corresponded to the mean value of the contiguous slices. All slices were normalized against the greatest intensity value of the corresponding MRI volume and cropped to a region of interest of 131 pixels $\times$ 256 pixels to reduce computational time.

3) Anisotropic Diffusion: In order to increase the brightness homogeneity within the vertebral bodies and preserve edges, we applied the anisotropic diffusion algorithm with adiabatic boundary conditions and exponential nonlinearity given in [7] to the intensity-corrected images. Fig. 3 shows an original image and its preprocessed version after coil-correction and anisotropic diffusion enhancement. In this paper, a different set of values for the anisotropic diffusion parameters λ, K, and number of iterations were used. The parameter λ controls speed of diffusion, and the maximum suggested value is 0.25. The parameter K controls conduction as a function of gradient. Small intensity gradients are able to block conduction and hence diffusion across step edges if K is low. A large value of K reduces the influence of intensity gradients on conduction, and as the number of iterations increases the scale becomes coarser.

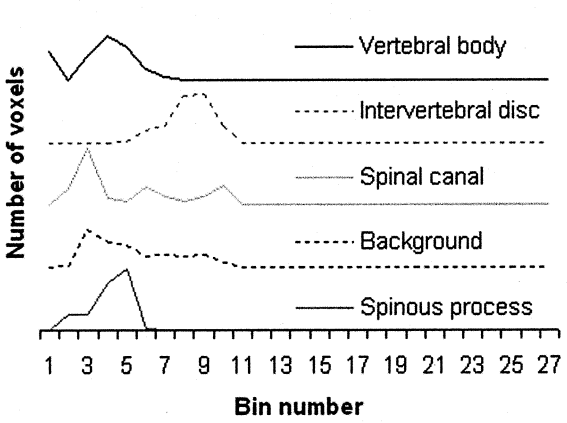

Fig. 4. Comparison between 3-D histograms of brightness for different voxels ($\lambda = 0.25, K = 10,$ number of iterations $= 5,$ rp $= 5,$ rz $= 5,$ number of bins $= 27$).

4) Three-Dimensional Local Histograms of Brightness: Although NCut readily admits combinations of different features, we decided to apply this segmentation technique taking 3-D local histograms of intensity as the segmentation feature based on preliminary results [9]. In [9], we also implemented NCut with the Nyström approximation method for the segmentation of vertebral bodies of sagittal T1-weighted images. However, the segmentation features were obtained in two dimensions: windowed histograms of brightness, or windowed histograms of textons with intensity and position. The selection of 3-D local histograms of brightness as the segmentation feature for this paper was done because we thought that a 3-D feature would increase robustness in the segmentation technique, and because of its computational simplicity compared with textons in three dimensions.

An anisotropic volume of rp voxels$\times$rp voxels (in plane)$\times$ rz voxels (through plane) centered on each voxel of the slice of interest, i.e., the noninterpolated slice that better showed the spinal canal, was used to calculate 3-D local histograms of brightness with nk bins. The bins were half-open intervals of width $1/(nk-1)$, where the kth bin was the half-open interval

$$\frac{k-1.5}{nk-1} \leq k\text{th bin} < \frac{k-0.5}{nk-1}. \tag{13}$$

A different number of bins and sizes of local volumes for the local histograms of brightness were experimented in this paper. Fig. 4 shows an example of 3-D local histograms of brightness for voxels corresponding to different anatomical structures of a sagittal T1-weighted MR image of the spine.

5) Normalized Cuts and the Nyström Approximation Method: In order to build the matrix (8) to solve the NCut problem through the Nyström approximation method, the local histograms of intensity were normalized and the χ^2 test, a simple and effective measure of histogram similarity [10], [11], was performed based on the previously random selection of m samples of 3-D normalized histograms

$$\chi^2(h_i, h_j) = \frac{1}{2}\sum_{k=1}^{nk}\frac{(h_i(k)-h_j(k))^2}{h_i(k)+h_j(k)} \tag{14}$$

where $h_i(k)$ is the number of voxels with brightness inside the range of the kth bin of the ith local histogram, i.e., the local histogram of the ith voxel. So each element of $\hat{\mathbf{W}}$ [shown in (8)] was written as

$$e^{-\frac{\chi^2_{ij}}{\sigma_{\chi^2}}} \tag{15}$$

where $\sigma_{\chi 2}$ is a parameter set up by the user to control the scale of the χ^2 test. Then we were ready to solve the eigenvector problem of the NCut technique through the Nyström approximation method [3]–[5]. This solution gave us as output m eigenvectors, where m was previously assigned as the number of random selected samples of 3-D normalized histograms of brightness. The number of elements of these eigenvectors equaled those of the original image, which means that each element of the eigenvectors could be mapped to one pixel in the image. The K-means clustering algorithm was applied to the eigenvector corresponding to the second smallest eigenvalue since it was expected that the Nyström approximation method gave a good estimate to the solution of the eigenvector problem of NCut. This eigenvector was clustered into three different groups to create three masks. In this paper, we applied a K-means function written in the C programming language based on the K-means function of Netlab toolbox [12]. Fig. 5 shows a coil-corrected image, its corresponding second eigenvector (according to the smallest eigenvalue) after the application of the segmentation procedure just described, K-means clustering of the second eigenvector into three groups, and the segmentation result.

6) Display: In order to display the segmented vertebral bodies, the original image was displayed and the user had to click twice at different positions over each vertebral body of interest. This step could be done at any stage of the segmentation procedure since this information is only used for displaying purposes. Based on the points selected by the user, the mask of the vertebral bodies of interest was extracted applying a 4-connectivity labeling technique to the group of the clustered data containing the vertebral bodies. A closing morphological operation was performed with a standard 3×3 isotropic kernel to the extracted mask before its application to the original slice to display the segmented vertebral bodies. All these operations were done taking advantage of built-in functions of the image processing toolbox of MATLAB (The MathWorks, Inc., Natick, MA).

IV. Results and Discussion

Six different experiments for each one of the six subjects were implemented in this study. The difference between experiments was based on the values of the different parameters that can be controlled:

1) Anisotropic diffusion: λ, K, number of iterations.
2) Three-dimensional local histograms of brightness: number of bins (nk) and size of the local volume to calculate the histograms (rp and rz).
3) NCut and Nyström approximation method: σ_{χ^2} and number of randomly selected samples (m).

Segmentation results of each one of the six experiments were quantitatively evaluated taking manual segmentation as reference. The measures for quantitative comparisons were area er-

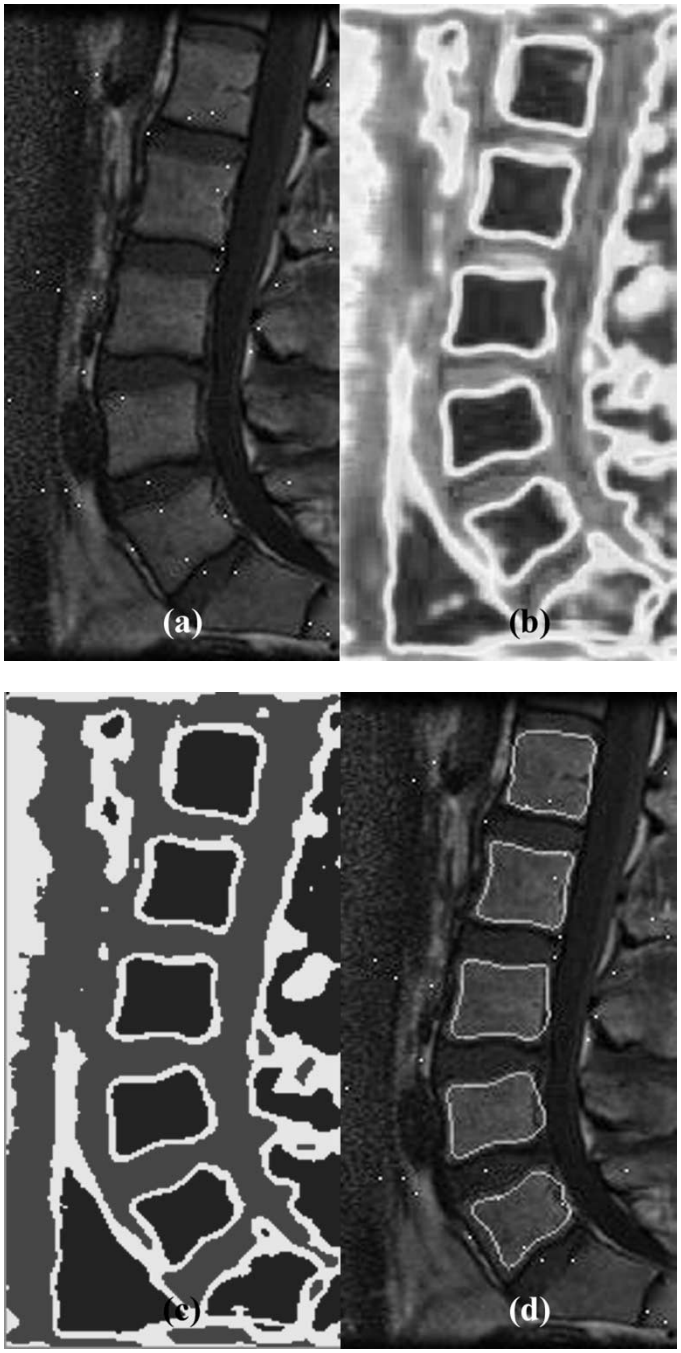

Fig. 5. (a) Coil-corrected image with random samples represented as white dots. (b) Second eigenvector according to the smallest eigenvalue. (c) K-means clustering (three groups, 100 iterations) of the second eigenvector. (d) Borders of NCut segmentation. Original image was cropped to reduce computational time.

rors, overlap area errors, and average distances. Table I summarizes these results, while Figs. 6 and 7 visually show some of them. The area and overlap area errors were defined as

$$\text{area error} = \frac{\text{nvoxelsNCut} - \text{nvoxelsManual}}{\text{nvoxelsManual}} * 100 \tag{16}$$

$$\text{overlap error} = 100 - \frac{\text{nvoxelsNCut}}{\text{nvoxelsCommon}} * 100 \tag{17}$$

where nvoxelsNCut is the total number of voxels classified as vertebral bodies by NCut, nvoxelsManual is the total number of voxels classified as vertebral bodies by manual segmentation, and nvoxelsCommon is the total number of voxels classified as vertebral bodies by both NCut and manual segmentation. In order to compute the average distances [13], the boundaries

TABLE I
COMPARISON OF MANUAL AND NCUT SEGMENTATION

Image	Area error (%)	Overlap area error (%)	Average distance (pixels)
Experiment 1. $\lambda = 0.25$, $\mathcal{K} = 10$, number of iterations = 5, rp = 3, rz = 3, number of bins = 27, nsamples = 34, $\sigma_{\chi 2} = 1$			
Subject1	-17.87	-2.09	4.01
Subject2	-9.74	-9.47	4.99
Subject3	-18.07	-1.89	3.93
Subject4	-23.73	-0.4	7.82
Subject5	-12.58	-3.08	4.99
Subject6	-4.62	-25.72	18.37
Mean	**-14.44**	**-7.11**	**7.35**
Standard dev.	**6.83**	**9.65**	**5.58**
Experiment 2. $\lambda = 0.25$, $\mathcal{K} = 10$, number of iterations = 5, rp = 3, rz = 3, number of bins = 50, nsamples = 75, $\sigma_{\chi 2} = 1$			
Subject1	-18.99	-2.04	4.37
Subject2	-8.66	-10.3	5.55
Subject3	-19.72	-1.72	5.85
Subject4	-24.53	-0.41	8.69
Subject5	-14.15	-3.02	6.69
Subject6	-11.88	-19.08	14.29
Mean	**-16.32**	**-6.1**	**7.57**
Standard dev.	**5.82**	**7.26**	**3.59**
Experiment 3. $\lambda = 0.25$, $\mathcal{K} = 10$, number of iterations = 5, rp = 5, rz = 7, number of bins = 27, nsamples = 34, $\sigma_{\chi 2} = 1$			
Subject1	-22.29	-2.23	5.29
Subject2	-15.06	-7.92	5.73
Subject3	-17.31	-4.32	5.08
Subject4	-27.2	-0.5	6.66
Subject5	-17.65	-2.68	5.72
Subject6	-12.12	-22.76	15.65
Mean	**-18.61**	**-6.74**	**7.36**
Standard dev.	**5.38**	**8.24**	**4.1**
Experiment 4. $\lambda = 0.25$, $\mathcal{K} = 10$, number of iterations = 5, rp = 5, rz = 5, number of bins = 13, nsamples = 34, $\sigma_{\chi 2} = 1$			
Subject1	-21.2	-2.15	4.75
Subject2	-14.85	-8.98	6.42
Subject3	-21.71	-2.14	5.22
Subject4	-24.3	-0.46	5.09
Subject5	-18.25	-2.13	6
Subject6	-15.69	-17.84	12.35
Mean	**-19.34**	**-5.62**	**6.64**
Standard dev.	**3.7**	**6.69**	**2.87**
Experiment 5. $\lambda = 0.25$, $\mathcal{K} = 50$, number of iterations = 5, rp = 5, rz = 5, number of bins = 27, nsamples = 34, $\sigma_{\chi 2} = 1$			
Subject1	-20.94	-2.14	4.73
Subject2	-11	-10.66	5.74
Subject3	-17.07	-4.17	4.81
Subject4	-26.63	-0.55	6.3
Subject5	-17.58	-2.41	5.9
Subject6	-9.16	-25.65	16.74
Mean	**-17.06**	**-7.6**	**7.37**
Standard dev.	**6.42**	**9.52**	**4.63**
Experiment 6. $\lambda = 0.25$, $\mathcal{K} = 50$, number of iterations = 5, rp = 5, rz = 5, number of bins = 27, nsamples = 34, $\sigma_{\chi 2}$ = standard dev. of **E** + standard dev. of **F**, which were defined in (8).			
Subject1	-21.05	-2.2	4.82
Subject2	-12.7	-9.7	5.65
Subject3	-16.8	-4.41	4.85
Subject4	-26.44	-0.6	6.09
Subject5	-16.8	-2.58	5.79
Subject6	-7.37	-26.69	17.27
Mean	**-16.86**	**-7.7**	**7.41**
Standard dev.	**6.58**	**9.82**	**4.86**

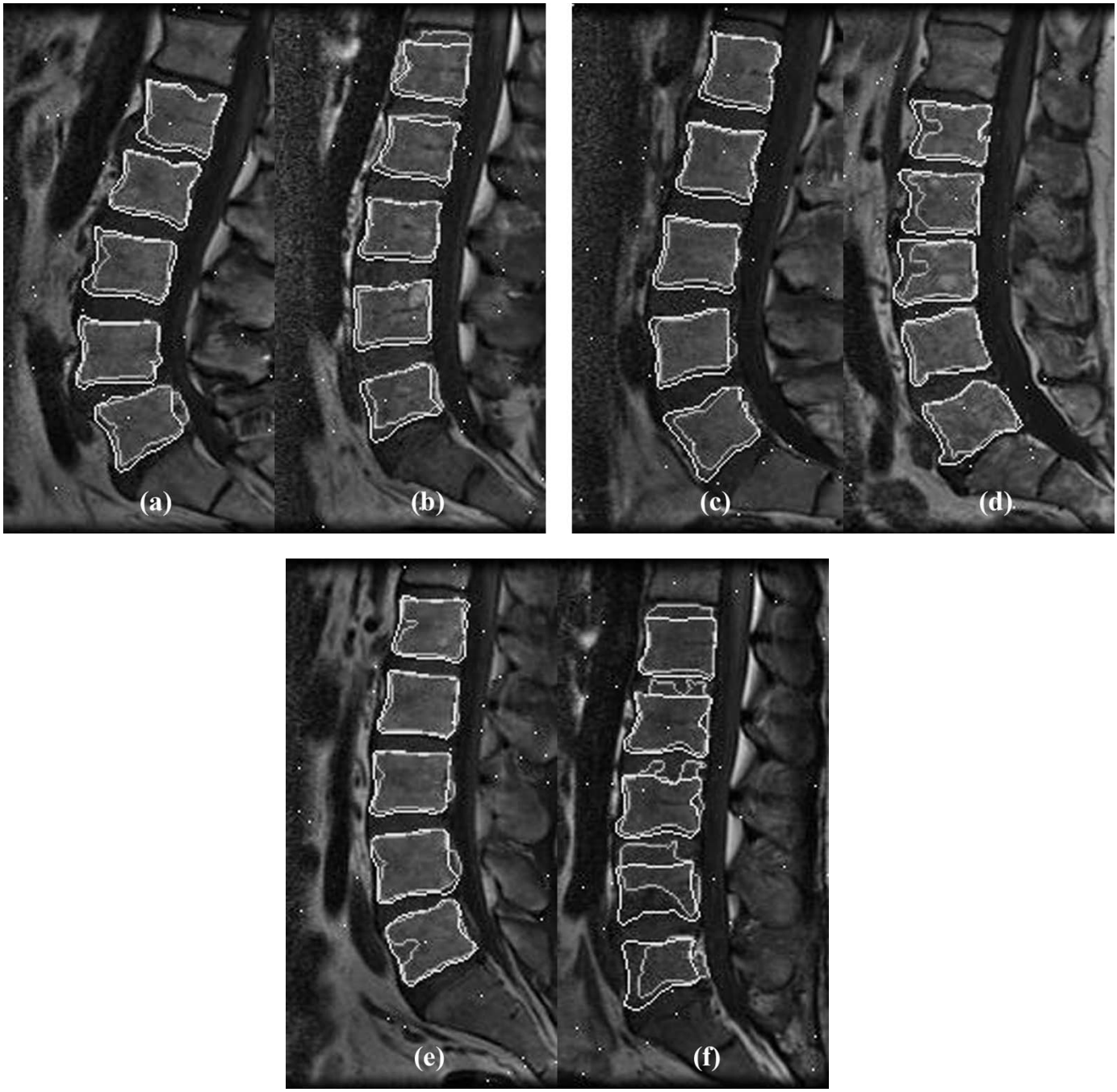

Fig. 6. Images of subject 1 (a), 2 (b), 3 (c), 4 (d), 5 (e), and 6 (f) corresponding to experiment 1 of Table I. White contours represent the boundaries of the manual segmentation, while gray contours those of NCut. The white dots represent the random samples selected for the segmentation procedure. Images were cropped to reduce computational time.

of the masks corresponding to the vertebral bodies segmented manually and by NCut were obtained by edge detection. Contours of corresponding vertebral bodies were matched and an artificial correspondence between their points was established finding the minimum distance between points on the matched curves. The average of these distances was considered as the average distance between the boundaries of manual segmentation and the boundaries of the mask obtained by NCut.

There are different interesting aspects to note from Table I. Results showed negative area errors in average, which means that vertebral bodies where smaller in area when segmented by NCut. The possible explanation for this effect is that edge pixels were not classified as vertebral bodies since edge pixels would have a different histogram pattern. In average the vertebral bodies segmented by NCut did not overlap the whole area of those segmented manually. However, this effect does not mean that the vertebral bodies segmented by NCut are inside the vertebral bodies segmented manually, although Figs. 6 and 7 qualitatively show that this was the dominant situation. In terms of average distances, values were high which translates in a necessity for improvement in the selection of features with the possible inclusion of region and edges information. It is important

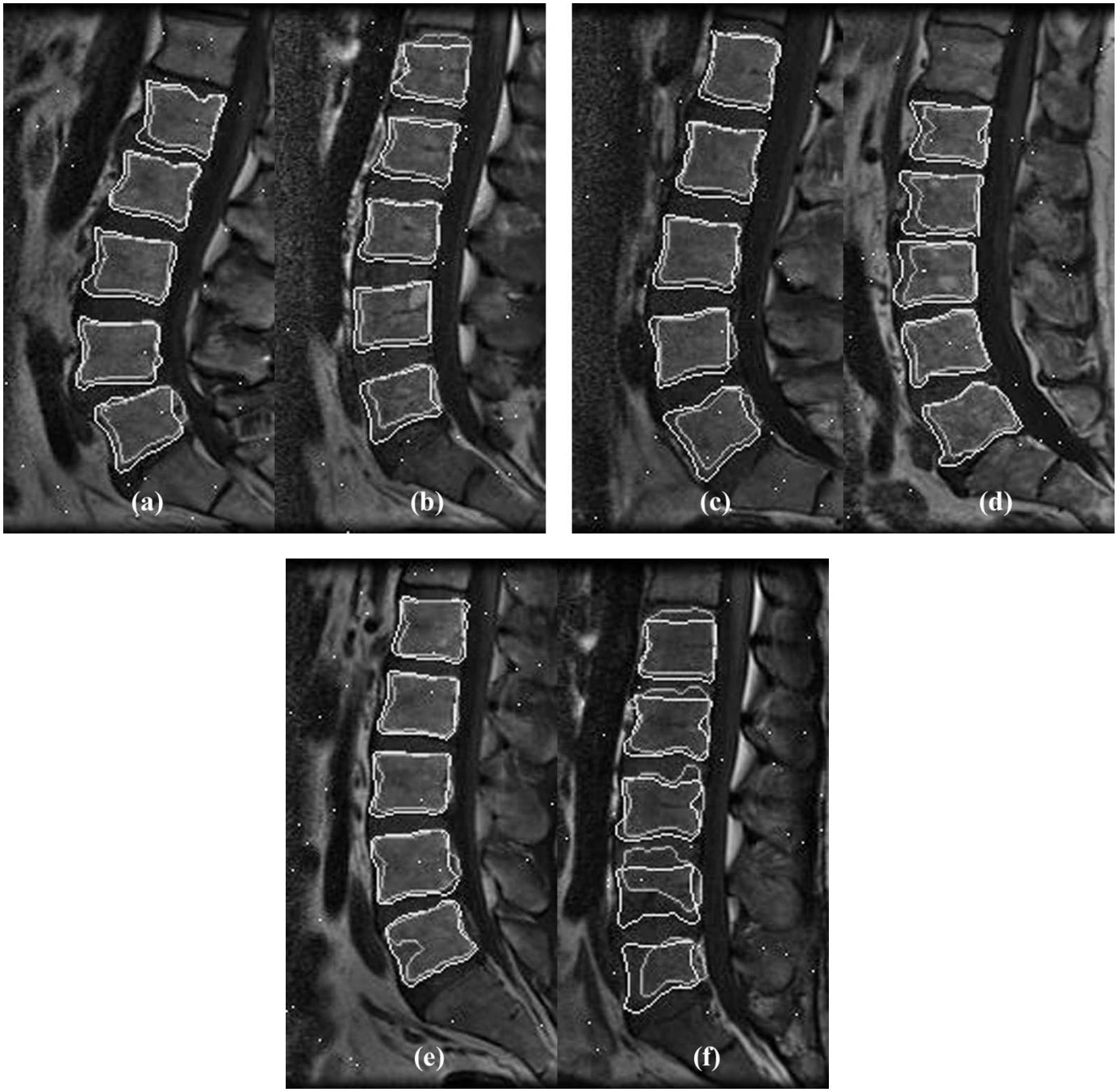

Fig. 7. Images of subject 1 (a), 2 (b), 3 (c), 4 (d), 5 (e), and 6 (f) corresponding to experiment 6 of Table I. White contours represent the boundaries of the manual segmentation, while gray contours those of NCut. The white dots represent the random samples selected for the segmentation procedure. Images were cropped to reduce computational time.

to note that NCut does not know anything about the shape or the intended group to be segmented. This is the main reason why we were not able to get the vertebral bodies from subject 6, which showed very little contrast between vertebral bodies and the rest of the anatomical structures. The design of coils with more homogenous reception profile and the improvement of coil correction algorithms are two viable options to increase contrast. This would also allow low-level segmentation algorithms such as NCut to take advantage of other segmentation features such as texture [9]. A different approach can also be taken through the application of segmentation techniques such as snakes (two-dimensional) or deformable models (3-D) that are able to include shape information as *a priori* knowledge for the segmentation task.

According to Table I, experiment 1 had the lowest mean area error, while experiment 4 had the biggest, although experiment 4 also showed the lowest mean overlap error and the lowest average distance. In addition to the parameters of the experiments shown in Table I, more combinations were tested. In general we found that for the anisotropic diffusion parameters, values bigger than 50 for K started to merge structures that were initially separated by a small gradient of brightness. This effect

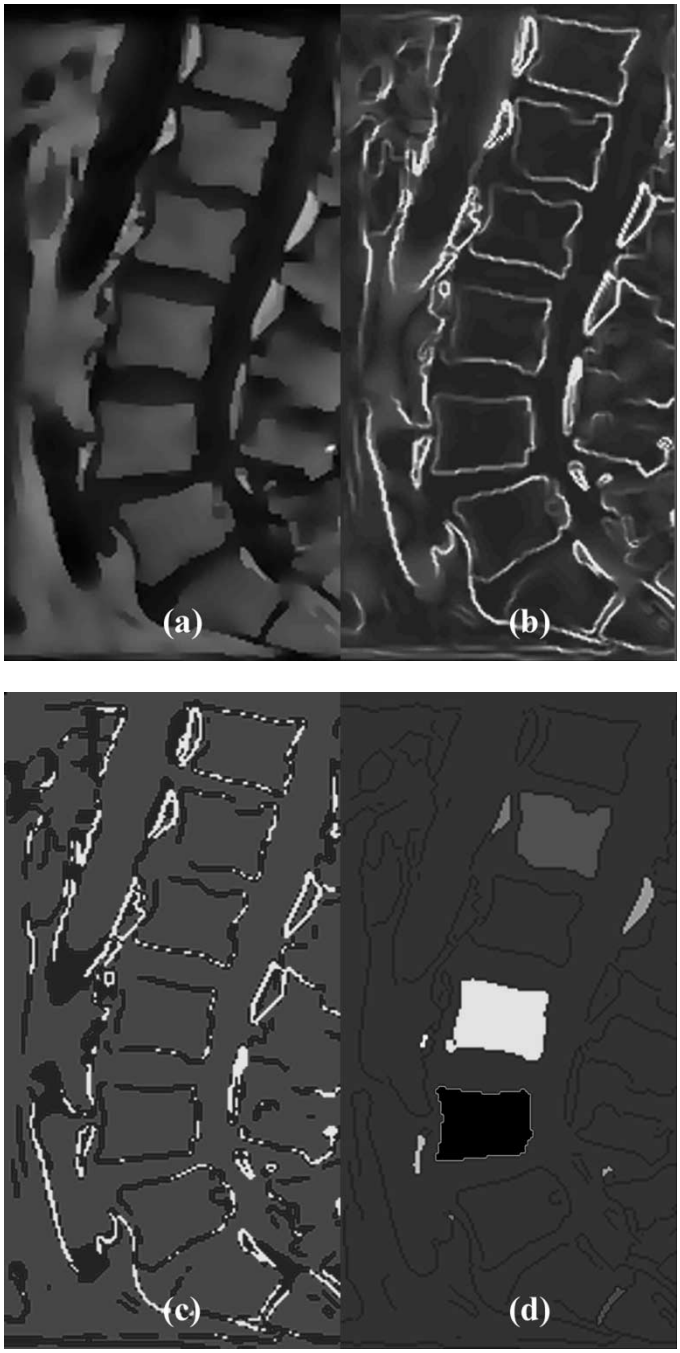

Fig. 8. (a) Image of subject 1 after coil-correction and anisotropic diffusion enhancement ($\lambda = 0.25, K = 50, \text{number of iterations} = 40$). (b) Magnitude of 3-D gradient of brightness of (a). (c) K-means clustering (3 groups, 100 iterations) of (b). (d) 4-connectivity labeling of the logical not of the edge map obtained for (a) by Canny edge detector in two dimensions ($\text{low threshold} = 0.0438, \text{high threshold} = 0.1094, \text{sigma} = 1$).

was expected as large values of K reduce the influence of intensity gradients on conduction. The number of iterations was kept low since we observed a similar effect than K at coarser scales. In terms of the 3-D local histograms of brightness, we found that values around 27 for the number of bins (chosen with the initial idea of calculating the local histograms in a anisotropic volume of 27 compartments), gave a good performance. The number of bins below 13 caused the vertebral bodies to appear with very different ranges of brightness in the eigenvectors. Values greater than 27 did not show any improvement. The number of randomly selected samples to solve the eigenvector problem through the Nyström approximation method showed a similar behavior to the number of bins. We choose 34 as the initial number of random samples ($\sim$0.001 the number of voxels in the cropped image). Values greater than 34 did not show any improvement, and values less than 20 showed variable behavior. The main reason is because samples were randomly selected, and reducing their number also reduced the possibilities that these samples corresponded to the most significant structures of the image. For σ_{χ^2} we also found a valid range of values 0.05–40. The effect of this factor, which we considered as the most sensitive, is better appreciated in the combination of different features, since it can be thought as a weighting factor.

In general, the algorithm performed well in those vertebral bodies showing high contrast with respect to the intervertebral discs and surrounding structures as shown in images of subjects 1–3, and some vertebral bodies of subjects 4 and 5 (Figs. 6 and 7). However, the performance was poor if this condition was not satisfied as in subject 6 (Figs. 6 and 7). Despite the fact that 3-D local histograms of brightness was used as the segmentation feature, the algorithm performance degraded when we tested far from the mid-sagittal slice, as the spinous processes show considerable heterogeneity and partial volume effects making the problem of segmentation very complex.

Although the objective was the segmentation of vertebral bodies from images acquired with protocols that are well established, such as T1-weighted, new MRI acquisition protocols could also enhance the contrast between bone and soft tissue to facilitate the segmentation task with low-level segmentation algorithms such as NCut or edge detection. The inability of the latter approach based on simple gradient of brightness or the Canny edge detector (Fig. 8) to segment the vertebral bodies was the main reason to explore NCut. However, results based on edge detection methods seem encouraging and we are looking to combine them with techniques that close small gaps of contours so we can perform the segmentation of the vertebral bodies and do a future comparison with NCut.

All segmentation by NCut was done in a laptop computer with an Intel Celeron processor, 995 MHz, 240 MB of RAM taking less than 1 min per image.

V. CONCLUSION

Accurate segmentation of vertebral bodies from MR images of the spine is still a task to be improved. In this paper we have shown that NCut combined with the Nyström approximation method provides promising segmentation results on MR images of the spine. We also have suggested different approaches that can be taken to improve the work presented in this paper.

Use of different image data sets such as combination of T1 and T2-weighted images, combining CT and MR images and segmented volumes will provide improved specificity particularly in multimodal registration, image-guided surgery applications, and the development of spinal models and atlases of spinal anatomy.

ACKNOWLEDGMENT

J. Carballido-Gamio would like to thank T. Dunn for his help in proofreading this paper.

REFERENCES

[1] S. Booth and D. A. Clausi, "Image segmentation using MRI vertebral cross-sections," in *Proc. Can. Conf. Electrical and Computer Engineering*, vol. 2, 2001, pp. 1303–1307.

[2] J. Shi and J. Malik, "Normalized cuts and image segmentation," *IEEE Trans. Pattern Anal. Machine Intell.*, vol. 22, pp. 888–905, Aug. 2000.

[3] C. Fowlkes, S. Belongie, and J. Malik, "Efficient spatiotemporal grouping using the Nyström method," in *Proc. CVPR*, vol. 1, Kauai, HI, 2001, pp. 231–238.

[4] C. Fowlkes, Q. Shan, S. Belongie, and J. Malik, "Extracting global structure from gene expression profiles," in *Methods of Microarray Data Analysis II*, S. M. Lin and K. F. Johnson, Eds. Norwell, MA: Kluwer Academic, 2002.

[5] S. Belongie, C. Fowlkes, F. Chung, and J. Malik, "Spectral partitioning with indefinite kernels using the Nyström extension," in *Proc. ECCV*, vol. 2, Copenhagen, Denmark, 2002, pp. 21–31.

[6] P. Perona and J. Malik, "Scale-space and edge detection using anisotropic diffusion," *IEEE Trans. Pattern Anal. Machine Intell.*, vol. 12, pp. 629–639, July 1990.

[7] P. Perona, T. Shiota, and J. Malik, "Anisotropic diffusion," *Geometry-Driven Diffusion Comput. Vis.*, vol. 1, pp. 73–92, 1994.

[8] L. Wald *et al.*, "Phased array detectors and an automated intensity-correction algorithm for high-resolution MR imaging of the human brain," *Magn. Reson. Med.*, vol. 34, p. 433, 1995.

[9] J. Carballido-Gamio, S. Belongie, and S. Majumdar, "NCut for spinal MRI segmentation," presented at the *CARS 2002*, Paris, France, 2002.

[10] J. Malik, S. Belongie, J. Shi, and T. Leung, "Textons, contours, and regions: Cue combination in image segmentation," presented at the *Int. Conf. Computer Vision*, Corfu, Greece, Sept. 1999.

[11] J. Puzicha, T. Hofmann, and J. Buhmann, "Non-parametric similarity measures for unsupervised texture segmentation and image retrieval," *Proc. IEEE Conf. Computer Vision and Pattern Recognition*, pp. 267–272, 1997.

[12] I. Nabney and C. Bishop. Netlab Neural Network Software. [Online]. Available: http://www.ncrg.aston.ac.uk/netlab/

[13] V. Chalana and Y. Kim, "A methodology for evaluation of boundary detection algorithms on medical images," *IEEE Trans. Med. Imag.*, vol. 16, Oct. 1997.